Temporal and spatial structure of phonon flux and induced drag currents in two-dimensional gases of electrons

B. A. Danilchenko
Institute of Physics of Ukrainian Academy of Sciences, Prospekt Nauki 46, 252650 Kiev, Ukraine

W. M. Gańcza and Cz. Jasiukiewicz
Institute of Theoretical Physics, University of Wrocław, pl. M. Borna 9, PL-50-204 Wrocław, Poland

T. Paszkiewicz
Institute of Theoretical Physics University of Wrocław pl. M. Borna 9, PL-50-204, Wrocław, Poland and Pedagogical University, ul. Rejtana 16A, PL-35-959 Rzeszów, Poland

(Received 1 March 1999)

We consider the response of a two-dimensional gas of electrons (2DEG) to pulsed beams of long-wavelength acoustic phonons in the time domain. The temporal and spatial structure of phonon fluxes is also studied. The results of computer experiments and numerical calculations, performed for 2D electrons lying on the (001) surface of a 2 mm thick GaAs platelet, indicate that for carefully chosen positions of 2D gas structure the induced drag current has the form of peaks of the opposite sign separated by a time interval approximately equal to 25 ns. These maxima are much stronger than the strongest amplitudes of current obtained in standard experiments on the integrated patterns of the drag currents. The spatial structure of these maxima indicates that by improving the time resolution one can work with quite large 2DEG structures. We expect that these strong phonon pulses can be used for studying nonequilibrium states 2D gases of carriers. [S0163-1829(99)12631-6]

I. INTRODUCTION

Beams of nonequilibrium phonons are widely used in studies of kinetic phenomena in phonon gases as well as in the investigations of kinetic phenomena in low-dimensional gases of carriers (LDGCs). In many such experiments strong anisotropy of phonon fluxes has been observed.[1] This phenomenon, called focusing of phonons,[2] has also been studied in computer experiments[3,4] and by means of numerical calculations.[5,6] Focusing of dispersionless acoustic phonons can be described in terms of elasticity theory[1,2] as well as of kinetic theory of phonons.[7,8]

The experiments of Karl *et al.* on phonon induced drag currents[9] have shown that low-dimensional gases of carriers [for example, 2D gases of electron (2DEG)] are sensitive to phonon wind. Nonequilibrium phonons induce drag currents which are related to quasimomentum transferred from these fluxes to LDGCs. Therefore, one may call LDGCs *phonon anemometers*. The corresponding theoretical description has been given in our previous paper.[10] In particular we showed that patterns of drag current are affined to quasimomentum focusing images.[10,11] Systems of excitons reacting to phonon pulses[12–14] (see also Ref. 1) provide another kind of phonon anemometer.

As a rule, results obtained for LDGCs are presented in the form of spatial maps of the time integrated drag currents. This integral drag effect provided some useful information about electron-phonon interaction. Together with energy focusing patterns[1,10] (obtained by means of detectors sensitive to the energy, i.e., bolometers), integral drag patterns comprise the set of spectroscopies of phonon images of crystals. A typical quasimomentum focusing pattern is shown in Fig. 1. Due to phonon focusing, this pattern is highly inhomogeneous and lines where quasimomentum density is large are called caustic lines. In the center of the pattern one sees a complicated ST-box structure (STB) of caustic lines.

In addition to phonon images, one can also study time-dependent response of bolometers[10] and anemometers.[15,16] Together with experiments on time dependent response of excitons,[1,14] these two types of measurements comprise the time-of-flight (TOF) spectroscopies. Since LDGCs are also sensitive to energy carried by beams of phonons, they are also used as bolometers.[17] Experiments of such kind provide useful and complementary information to this which can be extracted from drag currents.

The purpose of the present paper is to show that there exist crystalline directions and time windows for which am-

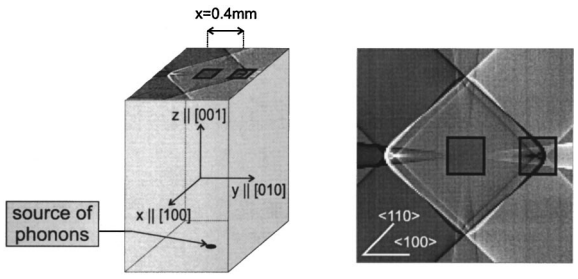

FIG. 1. (a) Schematic illustration of the experiment on phonon beams and (b) the map of the quasimomentum density obtained in computer experiments on a 2D electron gas lying in (001) lattice plane of GaAs. White lines denote positive and black, negative, whereas the gray regions correspond to the vanishing x component of quasimomentum density. Phonon anemometers are represented by shaded squares. One of them is placed in the center of ST-box structure (STB) opposite to the source and the other one covers one of the corners of STB.

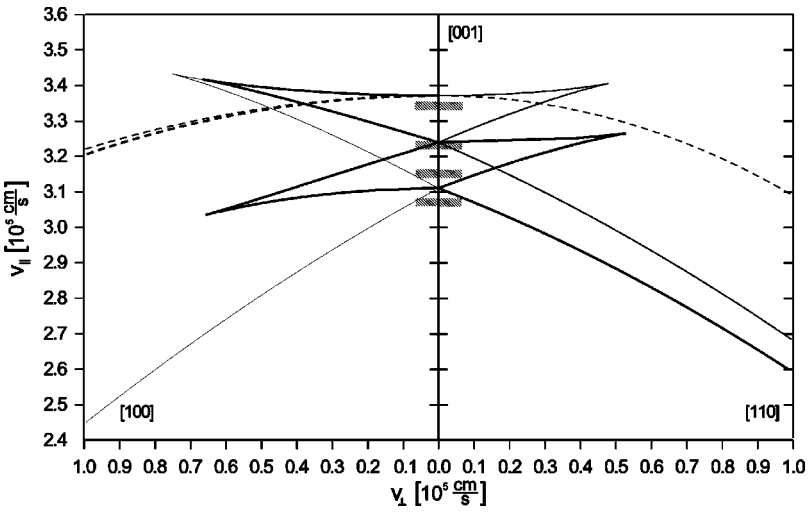

FIG. 2. Section of group velocity surfaces of TA phonons by plane in which the fourfold symmetry axis and respectively axes (a) [100] and (b) [110] are lying. The horizontal axis represents the values of $v_{g\perp}^{(j)}$, the vertical one, of $v_{g\parallel}^{(j)}$. Solid lines are STA modes, dashed lines are FTA modes. The experimental results obtained by Danil'chenko and Slutskii are indicated by horizontal bars, the widths of which are related to angle subtended by their detector.

plitudes of phonon fluxes and of the instantaneous induced drag currents are much stronger than for the corresponding time integrated drag currents and also to prove feasibility of such experiments. We expect that our findings may stimulate phonon studies of temporal evolution of nonequilibrium states of 2D gases of charge carriers.

All computer experiments presented here are performed using our program MCANSCAT (Monte Carlo anisotropic scattering).[18] This program can be treated as the extension of our two previous programs. One of them serves for the simulation of ballistic motion of long-wavelength acoustic phonons in cubic media,[4] while the other one simulates their propagation in isotropic media accounting for elastic scattering and down-conversion processes.[19] For numerical calculations we used our package of programs.[6]

II. PROPERTIES OF LONG-WAVELENGTH ACOUSTIC PHONONS

Since high-frequency phonons (in particular the optical phonons) generated by a source move with small group velocities and their lifetimes are short compared to long-wavelength acoustic phonons (LAPs) lifetimes, they have no chance to reach a distant detector. We shall neglect them, so here we consider only long-wavelength acoustic phonons, longitudinal (LA, $j=0$), and transverse (TA)—fast (FTA, $j=1$) and slow (STA, $j=2$).

A phonon carries the energy $\varepsilon_{\rm ph}=\hbar\omega$ and quasimomentum $\mathbf{p}_{\rm ph}=\hbar\mathbf{q}$. The energy $\varepsilon_{\rm ph}$ and, of course, the frequency ω, depend on the wave vector $\mathbf{q}$ and polarization j. For small wave vectors (obeying the inequality $qa\ll 1$, where a is the lattice constant and $q=|\mathbf{q}|$ is the length of $\mathbf{q}$), i.e., for LAPs, the dispersion law is linear in the magnitude of the wave vector

$$\omega(\mathbf{q},j)=c(\hat{\mathbf{q}},j)q, \quad (j=0,1,2). \tag{1}$$

We shall use the brief notation $\hat{Q}\equiv(\hat{\mathbf{q}},j)$.

The group velocity $\mathbf{v}_g(\hat{Q})=\partial\omega(\hat{Q})/\partial\mathbf{q}$ of a LAP wave packet with the mean wave vector $\mathbf{q}$ and polarization j propagating in an anisotropic medium has not, in general, the same direction as $\mathbf{q}$. It has the direction of the maximum rate of the frequency change and is perpendicular to the surface of constant frequency (ω surface) defined by the equation $\omega(\mathbf{q})=\omega_0$. For LAPs the group velocity $\mathbf{v}_g$ as well as the polarization vectors $\mathbf{e}$ also depend only on $\hat{Q}$. Direction $\hat{\mathbf{v}}_g$ of the group velocity is characterized by two angles—azimuthal θ_g and polar ϕ_g.

We calculated the group velocities for GaAs. In Fig. 2 we show two central sections of calculated group velocity surfaces of TA phonons obtained by two planes. The [001] axis is lying in both these planes. In one of them the axis [100] is lying, so this plane contains the center of STB side. In the other plane the axis [110] is lying, so it contains a corner of STB. On vertical axis the component $v_{g||}^{(j)}=v_g^{(j)}\cos\theta_g$ of $\mathbf{v}_g^{(j)}$ parallel to [001] axis is plotted, the perpendicular component $v_{g\perp}^{(j)}=v_g^{(j)}\sin\theta_g$ is plotted on the horizontal axes. Thick lines indicate several (degenerated) modes which propagate with the same group velocity (see Sec. ∇ B 1). Using these plots we calculated the dependency of arrival times on the shift along [100] and [110] axes, respectively (see Fig. 4). Cusps seen in Fig. 2 are cross sections of the folds of group velocity surfaces.[1] These folds correspond to parabolic lines on surfaces of constant frequency, along which ω surfaces are locally flat. Therefore, they are related to caustic directions along which fluxes of phonons are extremely large. Of course, in both real and computer experiments not all of these pulses can be resolved. The results of real-life experiments for velocities of propagation of phonon pulses[20] are shown in Fig. 2 by horizontal bars, their widths correspond to angles subtended by the detector used in these real-life experiments. Results of real-life experiments indicate that the time resolution of 25 ns can be achieved.[20]

Knowing the phase velocity $c(\hat{Q})$, one can introduce the slowness $s(\hat{Q})$, namely,

$$s(\hat{Q})=c^{-1}(\hat{Q}). \tag{2}$$

For each j the polar plot of the slowness, i.e., the plot of vectorial function $\mathbf{s}(\hat{Q})=\hat{\mathbf{q}}s(\hat{Q})$, gives the slowness surface (SLS). For LAPs an ω surface differs from the corresponding slowness surface only by a numerical factor

$$\mathbf{q}_{\omega_0}(\hat{\mathbf{q}},j)=\mathbf{s}(\hat{\mathbf{q}},j)\omega_0 \quad (j=0,1,2). \tag{3}$$

III. DENSITY OF ENERGY AND QUASIMOMENTUM FALLING ONTO A DETECTOR

Suppose that a crystalline specimen has the form of a platelet of the thickness d. Consider the experiment schematically shown in Fig. 1. A small source which radiates LAPs is located in the center of the Cartesian coordinate system with z, y, and x axes along [001], [010], and [100] crystalline directions, respectively. We assume that it radiates isotropically into the body angle 2π very short pulses of monochromatic phonons of the circular frequency ω (or of the linear frequency ν). For simplicity's sake, we assume that the probabilities to radiate a phonon belonging to LA, FTA, and STA branch do not differ.

The center of a movable and finite area detector (a bolometer or anemometer) is placed on the opposite side of the platelet at one of n_d selected points, say $\mathbf{r}_i=(r_i,\hat{\mathbf{r}}_i)=(r_i,\theta_r^{(i)},\phi_r^{(i)})$ $(i=1,\ldots,n_d)$. It is assumed that it has the form of a square with the side of a given length l_d. A wave packet of LAPs $(\hat{Q},\omega)$ moves across the medium with the group velocity $\mathbf{v}_g(\hat{Q})$.

Phonons, which reach the detector and are registered, have group velocities assembled around the vector $\mathbf{v}_g(\hat{Q})$ which satisfies two obvious geometrical conditions

$$\hat{\mathbf{v}}_g(\hat{Q})=\hat{\mathbf{r}}_i, \quad v_g^{(z)}(\hat{Q})>0. \tag{4}$$

The first condition can be written in a different form

$$\theta_g^{(j)}(\theta_q,\phi_q)=\theta_r^{(i)}, \quad \phi_g^{(j)}(\theta_q,\phi_q)=\phi_r^{(i)}, \quad 0\leqslant\theta_g^{(j)}<\pi/2. \tag{5}$$

For longitudinal LAPs $(j=0)$ ω surfaces are convex, so Eq. (4) [or (5)] has only one solution. In the case of transverse phonons ω surfaces consist of convex and concave regions as well as the parabolic lines. Hence, Eq. (4) has more than one solution, because generally particles populating different regions of the ω surface but with the same direction of $\hat{\mathbf{v}}_g$ may reach the bolometer (see Fig. 8). For each j and for a given detector position $\mathbf{r}_i$ we enumerate these solutions by the index w_i $(w_i=1,2,\ldots,n_i^{(j)})$. Thus, $\hat{\mathbf{q}}_j^{(w_i)}$ or $\theta_j^{(w_i)}$ and $\phi_j^{(w_i)}$ are the corresponding solutions.

Consider one of the branches of TA phonons (i.e., j is fixed). If $\hat{\mathbf{q}}_j^{(w_i)}$ points to a flat region of SLS, then there is a bundle of directions $\hat{\mathbf{q}}$ for which group velocity vectors are almost parallel to $\mathbf{r}_i$. Hence, the response of a finite area detector with the center placed at $\mathbf{r}_i$ should be very strong (i.e., phonons are focused).

The four position vectors pointing to corners of the detector placed at $\mathbf{r}_i$ $(i=1,\ldots,n_d)$ subtend the body angle $\Delta\Omega_i^{(r)}$. Only phonons having group velocity vectors with positive z components and belonging to this body angle may hit the detector. For each j to the body angle $\Delta\Omega_i^{(r)}=l_d^2/r_i^2$ (in the r space) there corresponds in q space one $(n_i^{(j)}=1)$ or more $(n_i^{(j)}\neq 1)$ bundles of phonon wave vectors $\Delta\Omega_q^{(j,w_i)}$. Therefore, for each j to the body angle $\Delta\Omega_i^{(r)}$ in q space there corresponds the total body angle $\Delta\Omega_q^{(j)}(\mathbf{r}_i)=\cup_{w_i=1}^{n_i^{(j)}}\Delta\Omega_q^{(j,w_i)}$.[6]

For chosen polarization j and position $\mathbf{r}_i$ of the detector we calculate the number of phonons $N_j(\mu,\mathbf{r}_i)$ reaching the detector during an interval of time $(t_\mu,t_{\mu+1})$. Calculating $E_j(\mu,\mathbf{r}_i)=\hbar\omega N_j(\mu,\mathbf{r}_i)$ and $E(\mu,\mathbf{r}_i)=\Sigma_{j=0}^2 E_j(\mu,\mathbf{r}_i)$ one obtains, respectively, partial, $E_j(\mu,\mathbf{r}_i)$, and total, $E(\mu,\mathbf{r}_i)$, energy densities carried by a monochromatic beam of phonons falling onto the detector placed at a selected position $\mathbf{r}_i$ and subtending the body angle $\Delta\Omega_i^{(r)}$ during the time interval $(t_{\mu+1},t_\mu)$.

Consider q_α, the αth component of the wave vector $\mathbf{q}$, and introduce in the q space a mesh characterized by δq

$$|q_\alpha^{(p+1)}-q_\alpha^{(p)}|=\delta q \quad (p=1,2,\ldots,n_q).$$

For each time interval $(t_\mu,t_{\mu+1})$ one can calculate $Q_\alpha^{(j)}(\mu,p;\mathbf{r}_i)$—the value of the α component of density of quasimomentum of phonons of jth kind with wave vectors belonging to the interval $(q_\alpha^{(p)},q_\alpha^{(p+1)})$ and falling onto the detector placed at $\mathbf{r}_i$ which subtends the body angle $\Delta\Omega_i^{(r)}$ during the time interval $(t_\mu,t_{\mu+1})$. Plots of $Q_\alpha^{(j)}(\mu,p;\mathbf{r}_i)$ will be termed the partial quasimomentum spectrograms for phonons of jth kind. The sum $\Sigma_{p=1}^{n_q}Q_\alpha^{(j)}(\mu,p;\mathbf{r}_i)$ gives $Q_\alpha^{(j)}(\mu;\mathbf{r}_i)$—the αth component of the density of quasimomentum carried by jth phonons falling onto the detector placed at the point $\mathbf{r}_i$ during the time interval $(t_\mu t_{\mu+1})$. Four sets of densities $E_j(\mu,\mathbf{r}_i)$ and $Q_\alpha^{(j)}(\mu;\mathbf{r}_i)$ provide, respectively, the energy and quasimomentum time-of-flight (TOF) spectrograms for the jth kind of phonons.

The αth component of the density of quasimomentum falling onto the detector placed at $\mathbf{r}_i$ and subtending the body angle $\Delta\Omega_i^{(r)}$ during the time interval $(t_\mu,t_{\mu+1})$ carried by acoustic phonons of all polarizations is $Q_\alpha(\mu;\mathbf{r}_i)=\Sigma_{j=0}^2 Q_\alpha^{(j)}(\mu;\mathbf{r}_i)$. Calculating the sum $\Sigma_\mu Q_\alpha(\mu;\mathbf{r}_i)$ we obtain αth component of total quasimomentum density $Q_\alpha(\mathbf{r}_i)$. The corresponding map is shown in Fig. 1.

Since we scored for all directions of wave vectors $\hat{\mathbf{q}}_j^{(w_i)}(\mathbf{r}_i)$ $(i=1,\ldots,n_d)$ pointing to neighborhoods of parabolic points, this method of calculating densities automatically accounts for the phonon focusing in the obtained TOF spectrograms and in the corresponding phonon images and is well suited for needs of computer experiments. The detailed description of the algorithm implemented in our program will be given in a forthcoming paper.[18]

IV. EXPERIMENTAL ARRANGEMENT

Real-life experiments on imaging and propagation of ballistic energy pulses in GaAs were performed by Eichele *et al.*[22] Slutskii and Danilchenko studied ballistic propagation of energy pulses.[20] Quasimomentum focusing patterns for GaAs were studied in our previous paper[10] by means of numerical calculations.

In our MC experiments on ballistic propagation of phonons in GaAs described here, they are sequentially generated by the source placed on (001) crystalline plane of a GaAs specimen (for which we have chosen the thickness $d=2$ mm which is characteristic for GaAs substrates used in MBE technology). We assume that the initial distribution of directions of phonon wave vectors is isotropic and that the probabilities to radiate a phonon LA, FTA, and STA do not

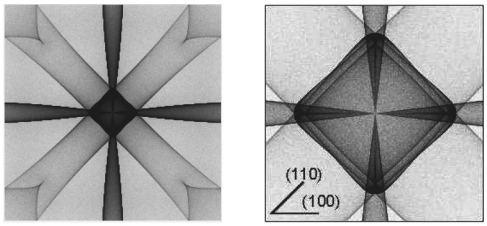

FIG. 3. (a) The map of the energy density obtained in computer experiments with a set of bolometers lying in (001) lattice plane of GaAs. (b) Caustic lines form the ''ST-box'' structure.

differ. The source is placed in the center of a Cartesian coordinate system. Its z axis is perpendicular to (001) plane in which lie the x and y axes. We chose a typical linear frequency $\nu=0.15$ THz. Bolometer or anemometer is placed on the opposite side of the platelet. In our computer experiments it has the form of the square of size $l=0.2$ mm, therefore it subtends angles $\Delta\phi_{\mathrm{det}}\lesssim 5.7°$.

Using the aforementioned program of MC simulations[18] we obtained the map of the total energy density $E(\mathbf{r}_i)$ falling onto specimen surface. In Fig. 3 one sees the caustic lines with STB encircling the pattern center (see also Fig. 1). This energy density map serves us as the reference pattern used in the computer experiments on the quasimomentum transport.

In the series of computer experiments on energy and quasimomentum carried by phonon beams, the detector was systematically shifted across the detector plane along a chosen axis $\hat{\mathbf{n}}$. As a result, the position of its center was scanned accordingly with the step which we chose to be equal to 0.1 mm. For the selected $\hat{\mathbf{n}}$ we performed computer experiments for 10 different positions of the detector. For the chosen two directions $\hat{\mathbf{n}}$ and the spatial step length this allowed us to cross the caustics lines forming STB.

If a phonon reaches the specimen boundary, the program MCANSCAT checks if it hits a detector placed at one of n_d selected positions, say $\mathbf{r}_i=(x_i,y_i,z=d)$. When the phonon strikes the detector, its characteristics are memorized and then analyzed.

V. RESULTS OF SIMULATIONS

A. Energy pulses

In Fig. 4 we show the *calculated* dependence of the arrival times of TA modes on the distance measured from STB center along axes [100] and [110], respectively, i.e., along directions pointing towards the related corner of STB and the center of suitable side, respectively. We discard LA modes, hence here pulses are formed by TA modes only. Points of caustic lines forming STB are related to cusps of lines depicted in Figs. 2 and 4. As it is seen in Fig. 4, for the used platelet, the caustic lines forming the corner and center of a side of STB are placed at the distance approximately equal to 0.4 and 0.3 mm, respectively.

To study time dependent fluxes of energy transported by phonons of a selected polarization j we shall calculate $E_j(\mu,\mathbf{r}_i)$. Typical pulses carrying energy obtained in our computer experiments are shown in Fig. 5 (upper curves in

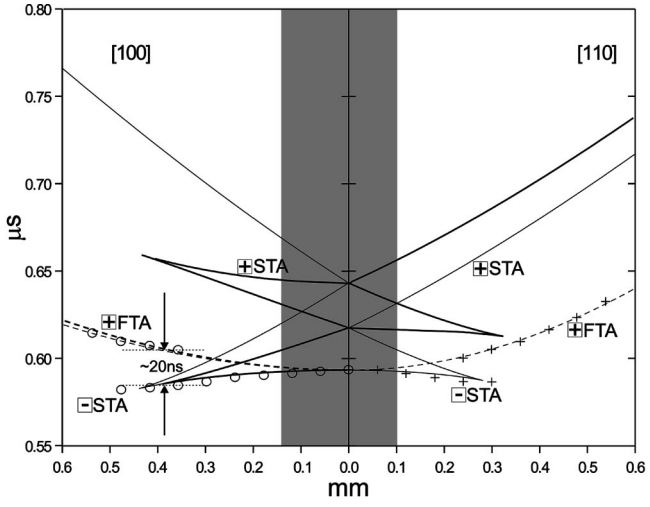

FIG. 4. Calculated dependence of TA modes arrival times on detector shift along [100] (left panel) and [110] axes (right panel). Solid lines: STA, dashed lines: FTA modes. Signs ahead of the mode indices mark the sign of x component of quasimomentum. Thick lines indicate several modes moving with the same group velocities. Detector placed in the STB center registers all modes arriving at various time instants within the shaded stripe. Daggers and circles denote results of computer experiments.

both panels). The analysis shows that the faster pulse is generated by STA phonons. The later pulse is formed by FTA phonons. Comparison of curves in the upper panel of Fig. 5 shows that for detector placed at STB center the x components of quasimomentum of arriving modes compensate.

For both shift directions and the detector center placed at STB center only the fastest (degenerated) and the slowest modes arrive as well separated peaks (see Fig. 4). The remaining modes form signals of rather complicated structure.

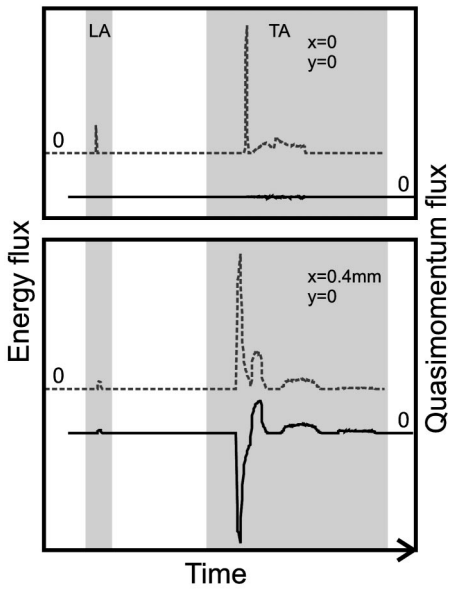

FIG. 5. Time-of-flight spectrograms obtained in computer experiments for conditions described in previous section. Detectors placed (i) in STB center (upper panel), (ii) at STB corner (lower panel). Upper curves: energy, lower curves: quasimomentum.

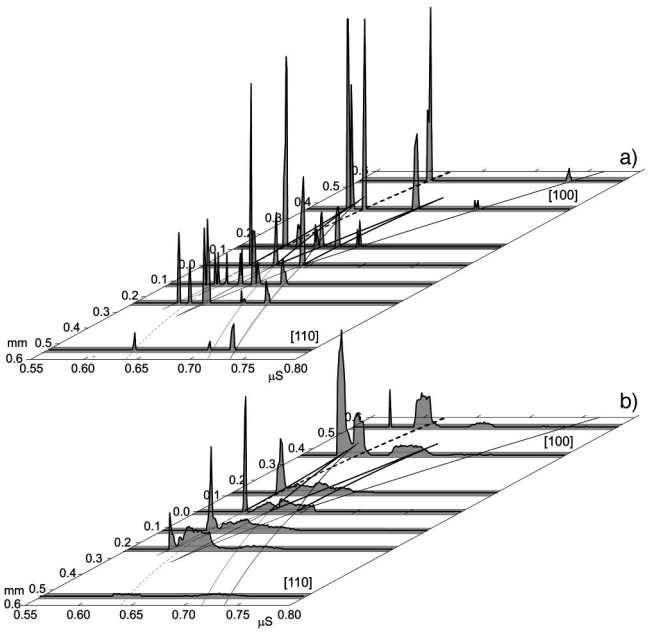

FIG. 6. Dependence of bolometer signal on time for various placements along [100] and [110] crystalline directions obtained in computer experiments. Detector area is (a) 0.02×0.02 mm^2, (b) 0.2×0.2 mm^2.

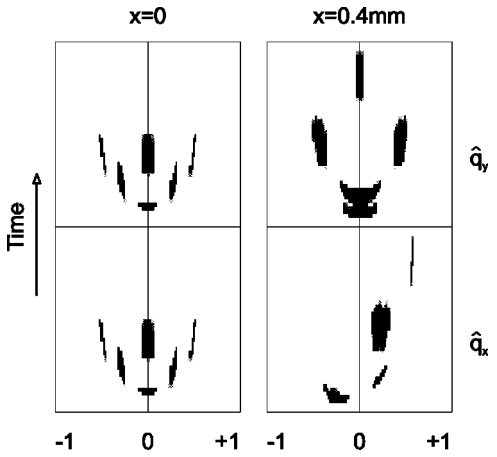

FIG. 7. Temporal quasimomentum spectrograms obtained in computer experiments: x and y components of wave vectors directions of TA phonons registered by two phonon anemometers placed in the center (left panel) and in the corner of STB lying on [100] axis (right panel).

The particular form of them depends on (i) the width of band of arrival times, (ii) the number of arriving phonons, and (iii) the extent of focusing or defocusing as well as on the degeneracy. This structure changes when detectors (i.e., the shaded stripe in Fig. 4) is shifted along one of chosen directions. Additionally, signals of detectors used in the real-life experiments are distorted by inertia. Hence, to obtain the actual phonon fluxes one should deconvolute observed detector signals.[21] Our results can be compared with the results of real-life experiments performed by Hübener and collaborators.[22]

Results of computer experiments for two sets of detector placements (along [100] and [110] directions) and for two detector areas are shown in Fig. 6. They present the time dependence of response of our ideal inertialess bolometer. Lines lying in the horizontal plane show the calculated spatial dependency of the arrival times (see Fig. 4). With the help of Fig. 6(a) one can study evolution of a small area bolometer signal with changing position. In the vicinity of folds signals are very strong, which reflects the focusing. Moving along lines one can observe the merging and splitting of pulses.

For a bolometer of bigger area only contributions of focused phonons are clearly seen and they arrive in the calculated instants of time. The remaining (sharp for small detector area) maxima now become rather broad. Generally, for such bolometers there is no simple relation between arrival times of their maxima and calculated arrival times.

B. TOF spectrography for quasimomentum

1. Partial quasimomentum spectrograms

As shown in Figs. 1 and 3, we have chosen $\hat{\mathbf{n}}=\hat{\mathbf{n}}_1 \equiv[100]$ and $\hat{\mathbf{n}}=\hat{\mathbf{n}}_2\equiv[110]$, i.e., the angles $\phi_r^{(1)}=0$, $\phi_r^{(2)}=\pi/2$. The detector placement in the (001) crystalline plane is characterized by the length l_i or by the azimuthal angle θ_i measured from the [001] axis. However, in this section we present only the results for two characteristic placements $\mathbf{r}_i$ of the detector: (i) $\mathbf{r}_i=\mathbf{r}_0$ ($x=0,y=0,z=2$ mm, or $x=l_0=0,\theta_r=0°$) and (ii) $\mathbf{r}_i=\mathbf{r}_{\mathrm{STB}}$ ($x=l_{\mathrm{STB}}\simeq0.4$ mm,$y=0,z=2$ mm, or $\phi_r=0°,\theta_r=\theta_{\mathrm{STB}}\simeq14.6°$). For the fixed source position and for the first placement, the detector is located in the center of STB. For the second one it covers the suitable corner of STB. Hence, for the second placement, it overlays several caustic lines.

In the first of two kinds of experiments on quasimomentum carried by phonon beams, we measured during various intervals of time the x and y components of in-plane components of wave vectors of arriving phonons. In this way we found the time dependence of q_x, q_y of these phonons. In the second kind of experiments, the total x component of the in-plane quasimomentum flux and the total flux of energy falling onto the specimen surface were studied.

As a result of the former kind of experiments, we obtained maps which we call *temporal quasimomentum spectrograms*. These spectrograms have the structure of ''clouds of spots.'' For $\hat{\mathbf{n}}=[100]$ and two selected detector placements the temporal quasimomentum spectrograms are shown in Fig. 7.

For the explanation of the obtained temporal quasimomentum spectrograms one should refer to Fig. 8 which schematically shows the central cross section (for $\phi_q=0$) of the slowness surface for STA mode. Let us recall that for a given propagation direction $\hat{\mathbf{q}}$, the group velocity vector $\mathbf{v}_g(\hat{Q})$ is perpendicular to the slowness surface at the point $\hat{\mathbf{q}}s(\hat{Q})$. Thus, the x components of quasimomenta of phonons with $\hat{Q}$'s corresponding to points a and a' (a and a' phonons) propagating along the fourfold axis have equal moduli but they are oppositely directed. The modes corresponding to the point b (b phonons) move in the same direction as a and a' phonons but, in agreement with Fig. 4, with a bigger group velocity. Therefore, phonons from a small neighborhood of

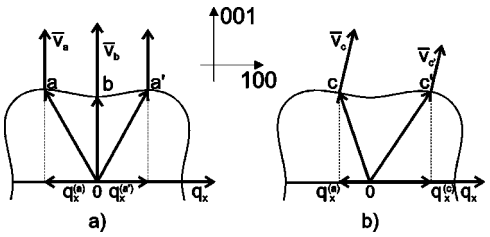

FIG. 8. A central section of the slowness surface of STA phonons propagating in GaAs. Two nonequivalent directions of the group velocity are chosen and the corresponding x components of the wave vectors are indicated.

the point b hit the detector before phonons from neighborhood of a and a'. Figure 8(a) shows that for b phonons the x components are concentrated in the vicinity of $q_x=0$, whereas x components of wave vectors of a and a' phonons are concentrated in the vicinity of $q_x\neq 0$ and are placed symmetrically with respect to the vertical axis. The remaining spots are due to remaining (oblique) modes fulfilling conditions (4). All phonons with wave vectors tipping points of the circle obtained by rotation of points a and a' around the vertical axis move with the same group velocity vectors, and arrive at the same detector in the same instant of time (they are ''degenerated,'' see Figs. 2 and 4, thick lines).

Assume that phonons are propagating in a direction slightly deviated from [001]. Then, to this direction there correspond two points c and c' of the ω surface which are placed nonsymmetrically with respect to the vertical axis. Since now group velocities and x components of the wave vectors of c and c' phonons are different, the spots pattern is nonsymmetric. Note that the central spot (corresponding to b phonons) is now absent. Since in Fig. 8(b) we changed only the x components of the group velocities, the pattern for y components remains symmetric. General situation is shown in Fig. 9.

This means that when the detector is placed in the center of STB the distribution of x and y components of quasimomentum flux of TA phonons is symmetric with respect to the horizontal axis ($q_x=0$, $q_y=0$, respectively) (Fig. 7, left panel). Therefore, for this placement of finite area anemometer, the positive and negative quasimomentum fluxes components compensate at any instant of time.

Notice that if the detector is placed near the caustic lines of STB, there arrive two kinds of TA phonons with opposite x components of the quasimomentum fluxes (see Fig. 7, right panel and Fig. 4, left panel). The related fluxes of different amplitudes arrive at different time instants, hence they do not mutually compensate and can be detected in TOF experiments. This situation is presented schematically in Fig. 8(b).

For directions far from STB, the mentioned peculiarities are not seen—the quasimomentum fluxes for TA and LA modes behave similarly, i.e., all x components have the same sign. We also calculated the corresponding matrix elements of the carrier-phonon interaction. For a small structure of 2D gas of carriers serving as the phonon anemometer placed at $\mathbf{r}_{\mathrm{STB}}$, these matrix elements are large, so the corresponding drag currents are also large. The numerical calculations described in Sec. VI B support this conclusion.

We studied also the propagation of pulses in Ge. Since the mass density and elastic constants of Ge and GaAs are very close, the obtained spot patterns resemble very much patterns obtained for GaAs. Energy density patterns for Ge were studied by Northrop and Wolfe.[23]

2. Quasimomentum pulses

Gaining some insight of properties of partial quasimomentum fluxes we are ready to calculate $Q_\alpha^{(j)}(\mu;\mathbf{r}_i)$, to analyze the corresponding TOF spectrograms, and compare spectrograms for energy and quasimomentum. For the two selected detector placements ($\mathbf{r}_0$ and $\mathbf{r}_{\mathrm{STB}}$), a typical quasimomentum pulse is displayed in Fig. 5 (lower curves). Since for both placements TA phonons are focused and move with markedly different group velocities, the bolometer response indicates at least one sharp maximum well separated from maxima which arrive later (Fig. 5, dotted lines). In agreement with Fig. 8(a), for $\mathbf{r}=\mathbf{r}_0$ the x component of quasimomentum flux (the solid line of the top panel of Fig. 5) is very small. For $\mathbf{r}_{\mathrm{STB}}$ the focusing yields strong quasimomentum fluxes of opposite signs which arrive at different instances of time. Inspecting the focusing pattern depicted in Figs. 1, 3, and 4, we conclude that these strong pulses of the opposite signs are related to the caustic lines of STB structure. From Fig. 4 it is seen that the negative pulse is due to the STA mode and the positive one to the FTA mode.

For the chosen thickness of the sample, the time interval separating negative pulse from the positive one is approximately equal to 25 ns, so they may be experimentally distinguished. Since the quantity which is studied in real experiments is the *density of induced current* not the *quasimomentum flux*, in the next section we consider response of 2D gas of electrons to pulses of bulk phonons moving in GaAs/GaAlAs heterostructure grown on (001) surface of 2 mm thick GaAs substrate.

Using our MC experimental data, we also obtained spectrograms of arrival times for pulses. They are shown in Fig. 4. As previously in these computer experiments a detector is shifted from the center of STB along (110) and (100) directions (crosses and circles, respectively). For the detector shifted along (100), we depicted results for two strongest TA peaks only. Group velocities of LA phonons are much bigger than of TA phonons and weakly depends on the direction of propagation, so we do not present them. Generally, group velocities of TA modes are more sensitive to the choice of the propagation direction than of LA mode. In agreement with Fig. 4, STA mode moving towards detector shifted along (110) direction disappears for the distance $l\simeq 0.3$ mm whereas in the case of the shift along (100) direction it still propagates for $0.3\lesssim l\lesssim 0.4$ mm. We shall mention that Lax *et al.* studied spectrograms of arrival times for the pulses of *short* wavelength acoustic phonons propagating in GaAs both in real[24] and Monte Carlo experiments.[25]

VI. RESULTS OF NUMERICAL CALCULATIONS FOR DRAG CURRENTS FOR HETEROSTRUCTURES

A. Characteristics of 2D gases of carriers

We shall briefly describe the properties of 2D gases of carriers (2DGC). Consider a 2DGC structure embedded in a specimen of a cubic medium of mass density ρ and volume

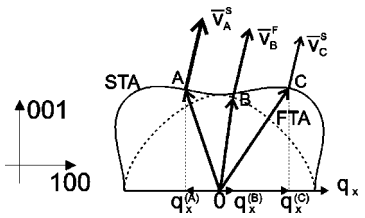

FIG. 9. Choice of direction of line joining the source and detector resulting in three groups of TA phonon wave packets moving in the same direction with different group velocities and q_x components (schematically). The STA A mode is focused, hence it yields the strongest maximum with $\hbar q_x^{(A)}<0$. The STA C mode is weakest because it is defocused and for it $\hbar q_x^{(C)}>0$. The FTA B mode gives the peak of intermediate strength which carries positive $\hbar q_x^{(B)}$. The thickness of arrows beginning at slowness surfaces indicates the strength of corresponding pulse, its length represents values of group velocities.

V. Assume that the carriers of the surface density n_s and the effective mass m^* occupy the lowest subband and that 2DGC fills a constriction parallel to a unit vector $\hat{\eta}$. Consider a carrier (electron or hole) with the wave vector $\mathbf{k}=\hat{\mathbf{k}}k=(k_x,k_y)$ and the energy $\varepsilon(\mathbf{k})$ and interacting with a bulk long-wavelength acoustic phonon of the polarization *j*, wave vector $\mathbf{q}=\hat{\mathbf{q}}q$, circular frequency $\omega(\mathbf{q},j)$, and the polarization vector $\mathbf{e}(\hat{\mathbf{q}},j)$.

As a result of scattering on acoustic phonon, the carrier wave vector $\mathbf{k}$ and energy $\varepsilon(\mathbf{k})$ change to $\mathbf{k}'$ and $\varepsilon(\mathbf{k}')$, respectively. The corresponding relaxation rate is proportional to $\Gamma_{q,j}(\mathbf{k},\mathbf{k}')$ (Ref. 11)

$$\Gamma_{q,j}(\mathbf{k},\mathbf{k}')=\frac{\hbar}{2\rho V\omega(\mathbf{q},j)}|F(q_z)|^2|M(\mathbf{q},j)|^2, \tag{6}$$

where $F(q_z)$ is the form factor which we take in the Howard-Fang form

$$F(q_z)=(1+aq_z)^{-3}, \tag{7}$$

and a is the effective thickness of 2DGC. The term $|M(\mathbf{q},j)|^2$ contains contributions of the deformation potential and piezoelectric interaction, namely,

$$|M(\mathbf{q},j)|^2=|\Xi_D\mathbf{e}(\hat{\mathbf{q}},j)\hat{\mathbf{q}}|^2+|2eh_{12}e_x(\hat{\mathbf{q}},j)\hat{q}_y\hat{q}_z+\hat{q}_xe_y(\hat{\mathbf{q}},j)\hat{q}_z+\hat{q}_x\hat{q}_ye_z(\hat{\mathbf{q}},j)|^2. \tag{8}$$

Introduce the ratio of the strength of piezoelectric coupling and the coupling constant of the deformation potential

$$\chi=\frac{2eh_{12}}{\Xi_D}. \tag{9}$$

TABLE I. Data used in numerical calculations.

n_s [cm^2]	m^* [m_e]	a [nm]	χ [m^{-1}]
5×10^{11}	0.067	4	4.143×10^8

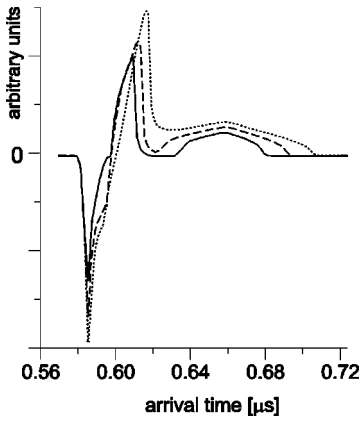

FIG. 10. Current induced by phonon pulses in a 2DEG placed at the corner of STB for various sides length l_d of a square detector. Solid line: $l_d=0.2$ mm, dashed line: $l_d=0.3$ mm, and the dotted line: $l_d=0.4$ mm. Calculations are performed for data described in previous sections.

In our computer experiments and numerical calculations we used typical data which we collected in Table I.

B. Spatial and temporal structure of the instantaneous drag currents

Using our package of programs[6] (see also Ref. 15), we calculated the dependence of the *x* component of the drag current on time for anemometer with the center position vector $\mathbf{r}=\mathbf{r}_{\mathrm{STB}}$. The results depicted in Fig. 10 agree quite well with TOF spectrograms obtained by means of Monte Carlo simulations. Namely, we observe two strong pulses of *drag current* induced by TA phonons moving with different group velocities. The contribution of LA phonons is negligible. The time interval between the arrival moments of the minimum and the fastest maximum is approximately equal to 25 ns. The fast STA pulse gives the negatively directed current, while the slower FTA induces the positively directed current. With increasing linear dimension l_d of the detector, the extrema become broader and higher. The drag current density averaged over time interval $\Delta t_s=(0.58\text{–}0.72)$ μs, where drag current does not vanish, constitutes 5–7 % of the maximal value of amplitude. This average corresponds to the intensity of caustics lines of the finite area phonon anemometer response map, i.e., to its strongest characteristics.[11,15] In agreement with Fig. 4, when the anemometer is placed on

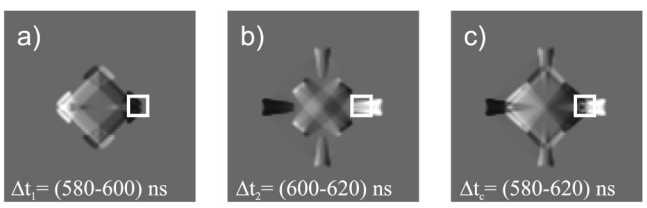

FIG. 11. Calculated spatial maps of amplitudes of the instantaneous drag current for various instants of time. The anemometer has shape of the square with 0.2×0.2 mm^2 sides with center placed at $\mathbf{r}_{\mathrm{STB}}$. Calculations are performed for data described in previous sections.

the right-hand side of STB, the negative pulse disappears and the amplitude of the positive one diminishes.

We also numerically obtained *spatial* maps of amplitudes of the *instantaneous* drag current for various instants of time (i.e., for short time intervals) when the center of phonon anemometer is placed at $\mathbf{r}_{\mathrm{STB}}$. Similar spatial maps of energy density can be obtained in real experiments.[26] Black and white points represent, respectively, large amplitudes of negative and positive drag current, the gray shaded regions correspond to the vanishing current. The square indicates 0.2×0.2 mm^2 anemometer with the center in the point P_a tipped by the vector $\mathbf{r}_{\mathrm{STB}}$. Figure 11 demonstrates the above map for three time windows $\Delta t_1=(580–600)$ ns, $\Delta t_2=(600–620)$ ns, $\Delta t_c=(580–620)$ ns.

Within time interval Δt_1, to the neighborhood of P_a there comes a group of STA phonons inducing a strong pulse of negative current. During the time interval Δt_2, strong and positive drag current is induced by FTA phonons. For both intervals the white and black structures are well separated, therefore for small enough detectors there is no averaging out of the signal. In the interval Δt_s the neighborhood of P_a is covered by these proximate white and black current structures which mutually compensate, so even for a small detector the signal becomes weaker. We see that experimental observation of large drag currents at selected instants of time is accessible and, unlike the spectroscopy of phonon images, the spatial resolution is not critical.

VII. CONCLUSIONS

We have shown that there exists at least four spatial directions and time window (for our platelet 0.58–0.60 μs) for which phonon fluxes are very strong. We focused our attention on GaAs and the direction defined by $\theta_{\mathrm{STB}}\approx14.7°$ and $\phi_{\mathrm{STB}}=0^0$. For these selected placements and chosen time window, the time depending density of the [100] component of quasimomentum falling onto anemometer consists of a sequence of strong negative (positive) and weaker positive (negative) pulses separated (for sample thickness $d=2$ mm) by the time $\Delta t\approx25$ ns. For other directions and different time windows this effect is not so pronounced. These pulses induce drag currents (or voltage) much stronger than those obtained in experiments with time integrated drag currents (i.e., when one deals with drag patterns).

In real-life experiments, applying electric or laser radiation pulses of large amplitudes, one can achieve strongly disturbed states of carrier gases. These disturbances can be correlated with the arrival times of the above described strong phonon pulses. Such pulses which induce intense drag currents, may probe nonequilibrium states of carriers. Thus, we expect that performing the corresponding real-life experiments, one may obtain the direct information about the interaction of low dimensional gases of carriers with acoustic phonons. We also plan to extend our studies of the properties of quasimomentum focusing to the case of the exciton system in Ge.[27]

[1] J. P. Wolfe, *Imaging Phonons* (Cambridge University Press, Cambridge, 1998).

[2] H. J. Maris, in *Nonequilibrium Phonons in Nonmetallic Solids*, edited by W. Eisenmenger and A. A. Kaplyanskii (North-Holland, Amsterdam, 1986), p. 52.

[3] A. G. Every, Phys. Rev. B **37**, 9964 (1988).

[4] W. M. Gańcza and T. Paszkiewicz, Comput. Phys. Commun. **85**, 423 (1995).

[5] G. A. Northrop, Comput. Phys. Commun. **28**, 103 (1982).

[6] Cz. Jasiukiewicz, T. Paszkiewicz, and D. Lehmann, Z. Phys. B **96**, 213 (1994).

[7] T. Paszkiewicz and M. Pruchnik, Physica A **232**, 747 (1996).

[8] T. Paszkiewicz and M. Wilczyński, in *Dynamical Properties of Solids*, edited by G. K. Horton and A. A. Maradudin (North-Holland, Amsterdam, 1995), Vol. 7, p. 250.

[9] H. Karl, W. Dietsche, A. Fischer, and K. Ploog, Phys. Rev. Lett. **61**, 2360 (1988).

[10] Cz. Jasiukiewicz, D. Lehmann, and T. Paszkiewicz, Z. Phys. B **84**, 73 (1991).

[11] Cz. Jasiukiewicz, D. Lehmann, and T. Paszkiewicz, Z. Phys. B **86**, 225 (1992).

[12] M. Greenstein and J. P. Wolfe, Phys. Rev. Lett. **41**, 715 (1978).

[13] L. V. Kieldysh and N. N. Sibeldin, in *Nonequilibrium Phonons in Nonmetallic Crystals*, edited by W. Eisenmenger and A. A. Kaplyanskii (North-Holland, Amsterdam, 1986), p. 455.

[14] A. V. Akimov, A. A. Kaplyanskii, E. S. Moskalenko, and R. A. Titov, Zh. Eksp. Teor. Fiz. **94**, 307 (1988) [Sov. Phys. JETP **67**, 171 (1988)].

[15] W. M. Gańcza, Cz. Jasiukiewicz, A. J. Kent, D. Lehmann, T. Paszkiewicz, K. R. Strickland, and R. E. Strickland, Semicond. Sci. Technol. **11**, 1030 (1996).

[16] Y. M. Kershow, S. J. Bending, W. Dietsche, and K. Eberl, Semicond. Sci. Technol. **11**, 1036 (1996).

[17] J. K. Wigmore, M. Erreol, M. Sahraoui-Tahar, C. D. W. Wilkinson, J. H. Davies, and C. Stanley, Semicond. Sci. Technol. **6**, 1030 (1996).

[18] W. M. Gańcza, I. A. Obukhov, T. Paszkiewicz, and B. A. Danilchenko (unpublished).

[19] B. A. Danil'chenko, D. V. Kazakovtsev, and I. A. Obkukhov, Zh. Eksp. Teor. Fiz. **106**, 1439 (1994) [Sov. Phys. JETP **79**, 777 (1994)].

[20] B. A. Danilchenko and M. I. Slutskii, Fiz. Tverd. Tela (Leningrad) **30**, 40 (1988) [Sov. Phys. Solid State **30**, 21 (1988)].

[21] S. C. Edwards, Hamid bin Rani, and J. K. Wigmore, J. Phys. E **22**, 582 (1989).

[22] R. Eichele, R. P. Hübener, and H. Seifert, Z. Phys. B **48**, 89 (1982).

[23] G. A. Northrop and J. P. Wolfe, Phys. Rev. B **22**, 6196 (1980).

[24] M. Lax, V. Narayanamurti, and R. Ulbrich, in *Phonon Scattering in Condensed Matter IV*, edited by W. Eisenmenger, K. Lassmann, and M. Dottinger (Springer, Berlin, 1984), p. 103.

[25] M. Lax, V. Narayanamurti, R. C. Fulton, and N. Holtzwarth, in *Phonon Scattering in Condensed Matter V*, edited by A. C. Anderson and J. P. Wolfe (Springer, Berlin, 1986), p. 335.

[26] M. E. Msall, Physica B **263-264**, 361 (1999).

[27] J. P. Wolfe, J. Lumin. **30**, 81 (1985).